Available online at www.sciencedirect.com
ScienceDirect
European Journal of Mechanics B/Fluids 27 (2008) 810–822

Rarefied gas flow in a triangular duct based on a boundary fitted lattice

Steryios Naris, Dimitris Valougeorgis *

Department of Mechanical and Industrial Engineering, University of Thessaly, Pedion Areos, Volos, 38334, Greece

Received 26 October 2007; received in revised form 3 January 2008; accepted 8 January 2008

Available online 16 February 2008

Abstract

The rarefied fully developed flow of a gas through a duct of a triangular cross section is solved in the whole range of the Knudsen number. The flow is modelled by the BGK kinetic equation, subject to Maxwell diffuse boundary conditions. The numerical solution is based on the discrete velocity method, which is applied for first time on a triangular lattice in the physical space. The boundaries of the flow and computational domains are identical deducing accurate results with modest computational effort. Results on the velocity profiles and on the flow rates for ducts of various triangular cross sections are reported and they are valid in the whole range of gas rarefaction. Their accuracy is validated in several ways, including the recovery of the analytical solutions at the free molecular and hydrodynamic limits. The successful implementation of the triangular grid elements is promising for generalizing kinetic type solutions to rarefied flows in domains with complex boundaries using adaptive and unstructured grids.

Keywords: Rarefied flows; Kinetic theory; Microflows

1. Introduction

Rarefied gas flows through channels of various cross sections have attracted, over the years, considerable attention by the research community. This interest is well justified due to the theoretical and practical importance of internal rarefied flows in several technological fields (e.g. vacuum technology, high altitude aerodynamics, nano- and microfluidics). Flow systems far from local equilibrium, with moderate or high rarefaction, can be treated in several ways including kinetic theory [1,2]. The main advantage of the kinetic approach is that the solution is valid in the whole range of the Knudsen number from the free molecular, through the transition and slip regimes all the way up to the hydrodynamic limit. In particular, when the flow is fully developed (linear), linearized kinetic theory is probably the most computationally efficient and accurate methodology to handle such flows.

A complete and thorough review of rarefied gas flows through channels of circular cross section, due to pressure and temperature gradients, is provided by Sharipov and Seleznev [3]. The implemented solution techniques include variational, moment and discrete velocity methods as well as semi-analytical approaches. The extension and application of all these techniques to flows through channels of non-circular cross sections is not trivial or straightforward

* Corresponding author.
E-mail address: diva@mie.uth.gr (D. Valougeorgis).

0997-7546/$ – see front matter
doi:10.1016/j.euromechflu.2008.01.002

since now the flow is not axisymmetric. Results for flows through channels of various cross sections, based on the integro-moment method, have been presented in the review article by Aoki [4], while more recently the discrete velocity method has been applied to solve flows through channels of orthogonal [5–7] and ellipsoidal cross sections [8]. Some of this work has been extended to binary gas mixtures by solving two coupled linearized kinetic equations [9,10].

However, as far as the authors are aware of, kinetic solutions for flows through channels of triangular cross sections, which are common in microchannels fabricated by silicon wet etching as well as in the vacuum pumping systems of fusion reactors, are not available. Also, when the discrete velocity method is applied to two or three dimensional problems the discretization in the physical space is always based on orthogonal cells. This is the main drawback when the method is applied to flow domains with complex boundaries. In the present work, some of these pitfalls are circumvented and the non-equilibrium flow of a gas through a triangular duct is solved by implementing for first time a triangular lattice. For this flow configuration the only available solutions are based on the Navier–Stokes equations subject to slip boundary conditions [11,12] and therefore the results are valid only in the slip regime. Here, the formulation, which is provided in Section 2, is based on the BGK kinetic equation [13] with Maxwell diffuse type boundary conditions and the results are valid in the whole range of the Knudsen number. The numerical scheme, described in Section 3, is based on a triangular lattice associated with the proper discretization of the kinetic equations in the physical and molecular velocity spaces. In Section 4, closed form solutions are provided at the free molecular and hydrodynamic limits. Results on the velocity profiles and on the flow rates in the whole range of gas rarefaction for ducts of various triangular cross sections are reported in Section 5. The accuracy of the results is validated in several ways, including the recovery of the analytical free molecular and hydrodynamic solutions at the two limits. Finally, some concluding remarks are given in Section 6.

2. Formulation

2.1. Flow configuration

Consider the rarefied flow of a gas through a long channel with length L, of constant triangular section, connecting two vessels maintained at pressures P_1 and P_2, with $P_1 > P_2$. The perimeter and the area of the cross section are defined by Γ' and A' respectively, while the hydraulic diameter of the channel, given by $D_h = 4A'/\Gamma'$, is taken as the characteristic macroscopic length of the problem. The flow configuration, the triangular cross section of the channel and the coordinate system with its origin are shown in Fig. 1.

The flow is considered as fully developed in the longitudinal direction and end effects in that direction are neglected. Therefore, the only non-zero component of the macroscopic velocity is the one in the z' direction and it is denoted by $u'(x', y')$. An other quantity of practical interest is the shear stress tensor, which has the non-zero elements $\Pi'_{xz}(x', y')$ and $\Pi'_{yz}(x', y')$ and their symmetric counterparts.

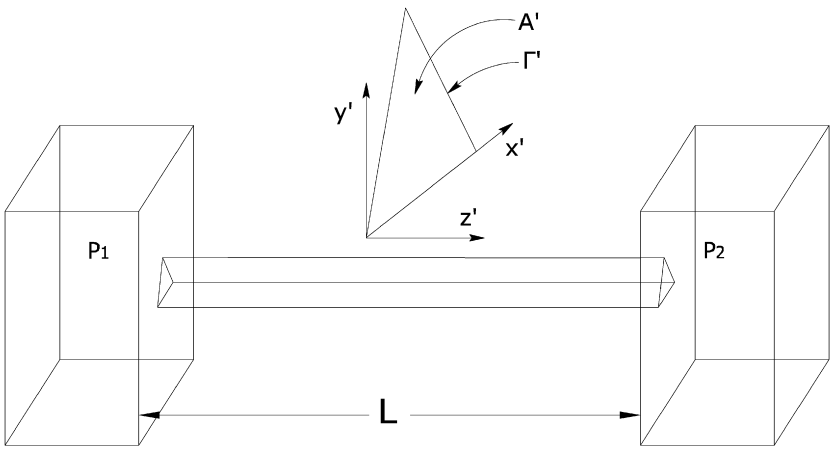

Fig. 1. Flow configuration and triangular cross section.

The characteristic parameter of the flow is the Knudsen number. However, for practical purposes related to the more comprehensive presentation of our results, we choose to use the so-called rarefaction parameter, defined as

$$\delta = \frac{D_h P}{\mu_0 v_0} = \frac{\sqrt{\pi}}{2}\frac{1}{Kn}. \tag{1}$$

Here, D_h is the characteristic macroscopic length, $P = (P_1 + P_2)/2$ is a reference pressure, μ_0 is the gas viscosity at reference temperature T_0 and $v_0 = \sqrt{2RT_0}$ is the characteristic molecular velocity, with $R = k/m$ denoting the gas constant (k is the Boltzmann constant and m the molecular mass). As it is seen the rarefaction parameter is defined in terms of measurable quantities and it is proportional to the inverse Knudsen number.

At this stage it is convenient to introduce the non-dimensional spatial variables $x = x'/D_h$, $y = y'/D_h$ and $z = z'/D_h$. In addition, we define the dimensionless area $A = A'/D_h^2$ and perimeter $\Gamma = \Gamma'/D_h$ of the cross section.

2.2. Kinetic equations

Since a kinetic approach is followed, the main unknown is the distribution function $f(\boldsymbol{r}, \boldsymbol{c})$, where $\boldsymbol{r} = (x, y)$ is the non-dimensional position vector, consisting only of two components since the flow does not alter in the z direction and $\boldsymbol{c} = (c_x, c_y, c_z)$ is the non-dimensional molecular velocity.

It has been shown that in the case of flows through long channels ($D_h \ll L$) the local pressure gradient, defined as

$$X_P = \frac{D_h}{P}\frac{dP}{dz'} = \frac{1}{P}\frac{dP}{dz} \tag{2}$$

is always small, independent of the pressure ratio P_1/P_2 [3,14]. Then, we may linearize the distribution function as

$$f = f^0\big[1 + X_P\big(h(x, y, \boldsymbol{c}) + z\big)\big] \tag{3}$$

where $X_P \ll 1$ is the local pressure gradient, while

$$f^0 = \frac{n_0}{(2\pi RT_0)^{3/2}}\, e^{-c^2} \tag{4}$$

is the global (absolute) equilibrium distribution function defined at reference number density n_0 and temperature T_0. The perturbed distribution function $h(x, y, c_x, c_y, c_z)$ obeys the two-dimensional linearized BGK equation [5]

$$c_x\frac{\partial h}{\partial x} + c_y\frac{\partial h}{\partial y} + \delta h = 2\delta c_z u - c_z, \tag{5}$$

where the quantity $u = u(x, y)$ at the right-hand side of Eq. (5), is the macroscopic velocity in the z direction and it is deduced by the first moment of h as

$$u(x, y) = \frac{u'}{v_0 X_P} = \frac{1}{\pi^{3/2}}\int_{-\infty}^{\infty}\int_{-\infty}^{\infty}\int_{-\infty}^{\infty} c_z h e^{-c^2}\, dc_x\, dc_y\, dc_z. \tag{6}$$

The validity of the BGK model for handling pressure driven isothermal flows has been verified in [3]. In particular, it has been shown that for flows through channels and tubes the discrepancy of the BGK model compared to other kinetic equations including the Boltzmann equation is within 2%. Therefore, it may be concluded that the present flow can be also tackled in a reliable manner using the simple BGK model equation. Of course this is not the case for temperature driven (non-isothermal) and/or concentration driven flows, where more advanced models are needed.

Another macroscopic quantity of practical interest is the non-dimensional shear stresses obtained by the second moments of h according to

$$\Pi_{xz}(x, y) = \frac{\Pi'_{xz}}{2PX_P} = \frac{1}{\pi^{3/2}}\int_{-\infty}^{\infty}\int_{-\infty}^{\infty}\int_{-\infty}^{\infty} c_x c_z h e^{-c^2}\, dc_x\, dc_y\, dc_z \tag{7}$$

and

$$\Pi_{yz}(x, y) = \frac{\Pi'_{yz}}{2PX_P} = \frac{1}{\pi^{3/2}}\int_{-\infty}^{\infty}\int_{-\infty}^{\infty}\int_{-\infty}^{\infty} c_y c_z h e^{-c^2}\, dc_x\, dc_y\, dc_z. \tag{8}$$

The gas-surface interaction is modeled by the Maxwell diffuse reflection condition. At the boundaries we have

$$f^+ = f(x, y, z, \boldsymbol{c}) = f_w^M \quad \text{for } \boldsymbol{c}\cdot\boldsymbol{n} > 0, \tag{9}$$

where $\boldsymbol{n}$ is the unit vector which is locally normal to the perimeter Γ, oriented toward the interior of A, while

$$f_w^M = \frac{n_w}{(2\pi RT_w)^{3/2}}\, e^{-(c-u_w)^2} \tag{10}$$

is the Maxwellian distribution with n_w, u_w and T_w denoting the corresponding wall quantities. In boundary condition (9), the distribution function f, corresponds to molecules departing from the walls and usually for simplicity in notation is denoted by f^+. Then, f^+ is linearized according to Eq. (3) as

$$f^+ = f^0\big[1 + X_P\big(h^+(x, y, \boldsymbol{c}) + z\big)\big], \tag{11}$$

where again h^+ denotes linearized distributions representing molecules departing from the boundaries. The Maxwellian f_w^M, given by (10), is also linearized with respect to f^0 using Taylor series and keeping terms up to first order we get

$$f_w^M = f^0(1 + X_P z). \tag{12}$$

This result is easily explained since the boundaries are isothermal and stationary. By substituting Eqs. (11) and (12) into Eq. (9) the linearized boundary condition

$$h^+ = h(x, y, \boldsymbol{c}) = 0 \quad \text{for } \boldsymbol{c}\cdot\boldsymbol{n} > 0 \tag{13}$$

along the perimeter Γ of the triangular duct is deduced.

The objective here is to solve the integro-differential equation (5), subject to boundary condition (13). At this stage it is convenient, by taking advantage of the two-dimensionality of the flow, to eliminate the c_z component of the molecular velocity vector by following the well-known projection procedure. Eq. (5) is multiplied by $\frac{1}{\sqrt{\pi}} c_z\, e^{c_z^2}$ and the resulting equation is integrated over all $-\infty < c_z < \infty$. The deduced equation after the projection does not contain the variable c_z and the computational effort associated with the implemented discrete velocity method, discussed in the next section, is significantly reduced.

Even more, for computational purposes it is convenient to express the two remaining components c_x and c_y of the particle velocity in terms of polar coordinates. The two-component dimensionless molecular velocity vector is now defined by its magnitude μ and its polar angle θ given by

$$\mu = \sqrt{c_x^2 + c_y^2} \quad \text{and} \quad \theta = \tan^{-1}\left(\frac{c_y}{c_x}\right) \tag{14}$$

respectively, where $0 \leqslant \mu < \infty$ and $0 \leqslant \theta \leqslant 2\pi$. In addition, using polar coordinates in the molecular velocity space we may write the linear differential operator acting on the distribution function at the left-hand side of Eq. (5) in the more convenient form

$$c_x \frac{\partial}{\partial x} + c_y \frac{\partial}{\partial y} = \mu\left[\cos\theta \frac{\partial}{\partial x} + \sin\theta \frac{\partial}{\partial y}\right] = \mu \frac{d}{ds}. \tag{15}$$

Here $s = s(x, y, \theta)$ denotes the direction of the characteristic line, which is passing from the point (x, y) and it is defined by the polar angle θ of the molecular velocity vector. A detailed presentation on the implementation of the polar coordinates and on the transformation of the differential operator may be found in [15].

Based on the above discussion we define the reduced distribution function

$$\phi(x, y, \mu, \theta) = \frac{1}{\sqrt{\pi}} \int_{-\infty}^{\infty} c_z h(x, y, \mu, \theta, c_z)\, e^{-c_z^2}\, dc_z, \tag{16}$$

and we operate accordingly on Eq. (5) to deduce, after some routine manipulation, the reduced BGK equation

$$\mu \frac{d\phi}{ds} + \delta\phi = \delta u - \frac{1}{2}. \tag{17}$$

By applying the corresponding reduction procedure to the non-dimensional macroscopic quantities, given by Eqs. (6)–(8), we find

$$u(x,y)=\frac{1}{\pi}\int_0^{2\pi}\int_0^{\infty}\mu\phi\, e^{-\mu^2}\,d\mu\,d\theta, \tag{18}$$

$$\Pi_{xz}(x,y)=\frac{1}{\pi}\int_0^{2\pi}\int_0^{\infty}\mu^2\cos\theta\,\phi\, e^{-\mu^2}\,d\mu\,d\theta \tag{19}$$

and

$$\Pi_{yz}(x,y)=\frac{1}{\pi}\int_0^{2\pi}\int_0^{\infty}\mu^2\sin\theta\,\phi\, e^{-\mu^2}\,d\mu\,d\theta. \tag{20}$$

The boundary condition for the reduced kinetic equation (17) is obtained by applying to boundary condition (13) the projection procedure followed by the change of the microscopic velocity variables from Cartesian to polar coordinates. Then, along the perimeter Γ of the channel we have

$$\phi^+=0 \tag{21}$$

where again the superscript $+$ denotes distributions, which represent reflected particles. The distributions, which represent molecules arriving at the boundaries are unknowns and are obtained as part of the solution.

2.3. Estimation of flow rate and mean wall shear stress

The mass flow rate through the channel is estimated by

$$\dot{M}=\iint_{A'}\rho(x',y')u'(x',y')\,dx'\,dy', \tag{22}$$

where the area A' of the triangular cross section and the macroscopic velocity $u'(x',y')$ have been defined before, while $\rho(x',y')$ is the local mass density. The double integral at the right-hand side of Eq. (22) is non-dimensionalized and by using the equation of state $P=\rho RT_0=\frac{1}{2}\rho v_0^2$ we define the non-dimensional flow rate

$$G=\frac{\dot{M}v_0}{A'PX_P}=\frac{\dot{M}v_0}{A'D_h\frac{dp}{dz'}}=\frac{2}{A}\iint_A u(x,y)\,dx\,dy. \tag{23}$$

Once the kinetic problem, described by Eq. (17) and boundary condition equation (21) is solved, the macroscopic velocity u is computed from Eq. (18) and then non-dimensional flow rate G is readily deduced from the double integral in Eq. (23). It is seen that G depends only on the rarefaction parameter δ and on the dimensionless area A of the cross section. In Section 5, tabulated results for G in terms of δ are presented, for various triangular cross sections A.

The mean wall shear stress is defined as

$$\bar{\tau}_w'=\frac{1}{\Gamma'}\int_{\Gamma'}\Pi'\,dt' \tag{24}$$

where Γ' is the perimeter of the cross section of the channel and Π' is the shear stress along the wall, while t' denotes the integration variable. Based on basic principals [16] and by introducing the non-dimensional quantities we find [17]

$$\bar{\tau}_w=\frac{\bar{\tau}_w'}{2P_0X_P}=\frac{1}{\Gamma}\int_{\Gamma}\Pi\,dt=\frac{A}{2\Gamma}=\frac{1}{8}. \tag{25}$$

Here, $\bar{\tau}_w$ is the non-dimensional mean wall shear stress, while Π is obtained by a linear combination of Π_{xz} and Π_{xy}, given by Eqs. (19) and (20) respectively, along the dimensionless perimeter Γ. As it has been shown recently for any cross section $\bar{\tau}_w$ is independent of the rarefaction parameter δ and it is equal to the ratio $A/(2\Gamma)$, which since we are using the hydraulic diameter as the characteristic macroscopic length, it is always equal to 0.125 [17]. This finding is used in Section 5, as a benchmark, to test the accuracy of the kinetic calculations.

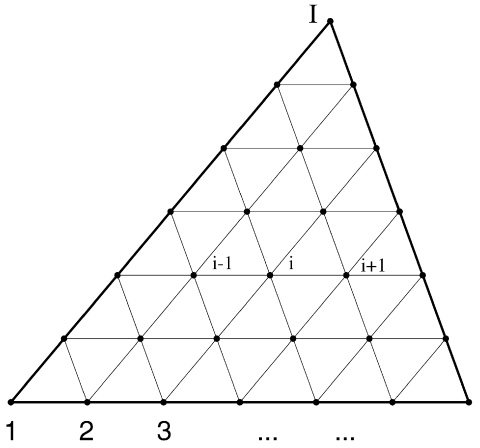

Fig. 2. Physical lattice with its triangular elements.

3. Numerical scheme

The computational approach for solving the linear integro-differential equation (17), supplemented by the corresponding integral expression (18), is presented. First the two equations are discretized properly in the phase space and then their discretized versions are solved numerically in an iterative manner. The phase space is consisting of the molecular velocity space (μ, θ) and the physical space (x, y).

In the molecular velocity space the discretization is performed by choosing a suitable set of discrete velocities (μ_m, θ_n), defined by $0 \leqslant \mu_m < \infty$ and $0 \leqslant \theta_n \leqslant 2\pi$, with $m = 1, 2, \ldots, M$ and $n = 1, 2, \ldots, N$. The resulting set is consisting of $M \times N$ discrete velocities. By performing this discretization in the velocity space, Eq. (17) is reduced to a set of ordinary differential equations of the form

$$\mu_m \frac{d\phi_{m,n}}{ds} + \delta\phi_{m,n}(x, y) = \delta u(x, y) - \frac{1}{2}, \tag{26}$$

where the integral expression (18) for u is replaced by the double summation

$$u(x, y) = \frac{1}{\pi} \sum_m \sum_n w_m w_n \phi_{m,n}. \tag{27}$$

The Gauss quadrature has been used in the μ variable and the trapezoidal rule in the θ variable, while w_m and w_n are the corresponding weighting factors.

Next, the discretization in the physical space (x, y) is performed by dividing the flow domain in equal triangular elements. The grid is constructed by drawing inside the triangular cross section three groups of parallel lines. The lines of each group are equally distanced and parallel to one of the three sides of the triangle. The physical lattice with the equal triangular elements and their nodes i, with $i = 1, 2, \ldots, I$ are shown in Fig. 2. The benefits of such a discretization is obvious since the boundaries of the computational domain are identical to the boundaries of the triangular cross section of the channel, providing good accuracy in the numerical solution.

The system of ordinary differential equations (26) is discretized at each grid point i in the physical space yielding a set of algebraic equations. The first order derivatives with respect to s in Eq. (26), are approximated by a finite difference first order upwind scheme. To clearly demonstrate this procedure a detail of the physical lattice is presented in Fig. 3, where a typical node i, denoted by the letter K, and its six surrounding nodes, denoted by the letters A through F, are shown. The hexagonal $ABCDEF$ may be considered as the computational cell of the interior node K. Similar hexagonal computational cells exist for all interior nodes of the triangular computational domain. Now, in order to approximate the derivative $d\phi_{m,n}/ds$ at point K for the group of discrete velocities crossing the side AB of the hexagonal cell, we write

$$\mu_m \left.\frac{d\phi_{m,n}}{ds}\right|_K = \mu_m \frac{\phi_{K,m,n} - \phi_{N,m,n}}{\Delta s_{KN}}, \tag{28}$$

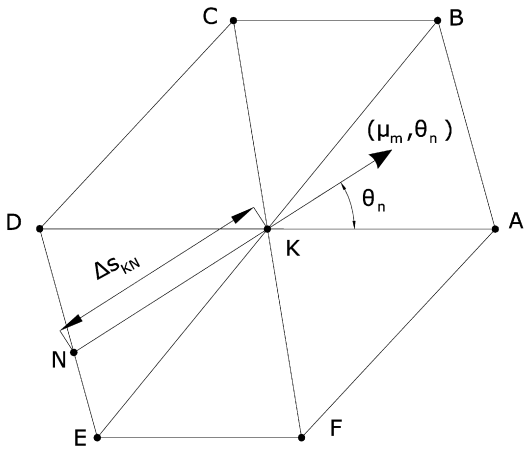

Fig. 3. Hexagonal computational cell and finite differencing along a characteristic.

where the point N and the corresponding distance Δs_{KN} are also shown in Fig. 3. Then, the quantities at point N are substituted by the corresponding quantities at the two adjacent grid points D and E using linear interpolation. This approach can be easily extended for values of the polar angles θ_n crossing the other five sides of the hexagonal and then it is repeated for all hexagonal computational cells. Overall, there are MxN equations at each of the I nodes.

As it has been pointed out the whole problem is solved in an iterative manner between the kinetic equation for ϕ and the integral expression for u. The iterations start by assuming some initial values in u. At each iteration the system of algebraic equations deduced by the kinetic equation is solved by a marching scheme. For each discrete velocity (μ_m, θ_n) the distribution function $\phi_{m,n,i}$ is computed explicitly marching through the physical lattice. The marching process starts always from the boundary and its direction depends upon the polar angle θ_n. Following this procedure no matrix inversion is required. Then, based on $\phi_{m,n,i}$ the macroscopic velocity u_i is computed by numerical integration. The new values of u_i are plugged back into the kinetic equation and the iterative procedure is ended when the imposed termination criterion on the convergence of u_i is satisfied. Following the above procedure, supplemented by a reasonable dense triangular grid and an adequate large set of discrete velocities we are able to obtain grid independent results with modest computational effort.

The discretization with the triangular boundary-fitted grid elements in the physical space, associated with the proper implementation of the discrete velocity method, is performed, as far as we are aware of, for first time in kinetic calculations.

4. Solutions at the free molecular and hydrodynamic limits and in the slip regime

In the free molecular limit ($\delta = 0$), the integro-differential equation (17) is reduced to a first order ordinary differential equation

$$\mu \frac{d\phi_{fm}}{ds} = -\frac{1}{2}, \tag{29}$$

subject to boundary condition (21). Here, ϕ_{fm} denotes the distribution function at the free molecular limit. This problem is solved analytically by integrating along the characteristics to yield a closed form solution for the distribution function

$$\phi_{fm}(x, y, \mu, \theta) = -\frac{s_0}{2\mu}. \tag{30}$$

The distance $s_0 = s_0(x, y, \theta) = x\cos(\theta) = y\sin(\theta)$, shown in Fig. 4, is the segment along the characteristic line defined by the angle θ, in the direction opposite to that of the molecular velocity (μ, θ), from the point (x, y) to the

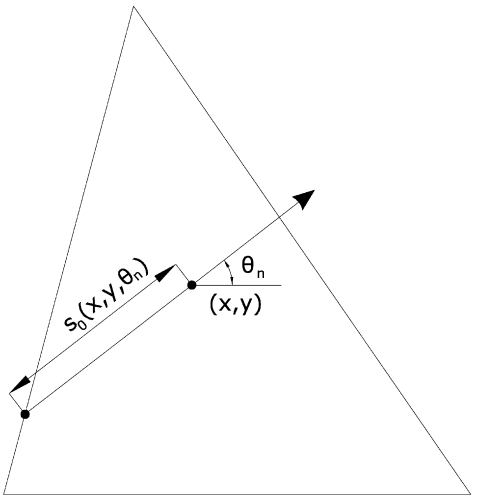

Fig. 4. Definition of distance $s_0(x, y, \theta_n)$.

boundary point where the characteristic is crossing the perimeter. Then, by substituting Eq. (30) into Eq. (18) we deduce

$$u_{fm}(x, y) = \frac{1}{4\sqrt{\pi}} \int_0^{2\pi} s_0(x, y, \theta)\, d\theta. \tag{31}$$

It is seen that at the free molecular limit, the estimation of the macroscopic velocity requires only the computation of the distances s_0 at each point (x, y) and for each polar angle θ, followed by a straight forward integration. Therefore, we consider this solution and the resulting non-dimensional flow rate G_{fm} as semi-analytical.

In the slip regime, fully developed flows through ducts of triangular cross sections may be obtained numerically, with small computational effort, by solving a Poisson equation for the unknown macroscopic velocity distribution subject to slip boundary conditions [12]. In terms of the dimensionless variables of our work, the problem is reduced to the one of solving the partial differential equation

$$\frac{\partial^2 u_s}{\partial x^2} + \frac{\partial^2 u_s}{\partial y^2} = -\delta, \tag{32}$$

in the area A, subject to the mixed boundary conditions

$$u_s = \frac{\sigma_P}{\delta} \frac{\partial u_s}{\partial n}, \tag{33}$$

on the perimeter Γ. The subscript s has been included in order to distinguish this solution, which is valid only in the slip regime, from the kinetic solution which is valid in the whole range of rarefaction. In Eq. (33), $\sigma_P = 1.016$ is the so-called velocity slip coefficient estimated by kinetic theory [3] and n denotes the inward normal direction to the surface.

In the specific case of an equilateral triangular cross section, the above problem described by Eqs. (32) and (33) has been recently solved analytically [11]. In terms of our variables, the closed form expressions for the velocity profile and the flow rate, given in [11], read

$$u_s(x, y) = \frac{\delta}{2(1 + 2\sigma_P/\delta)} \left[\left(\sqrt{3}xy - x^2 y + \frac{1}{3} y^3 - y^2 \right) + \frac{\sigma_P}{\delta} \left(\sqrt{3}x - x^2 + y - y^2 + \frac{\sigma_P}{\delta} \right) \right] \tag{34}$$

and

$$G_s = \frac{3\delta}{40} + \frac{\sigma_P}{5} \left(3 - \frac{\sigma_P}{\delta + 2\sigma_P} \right) \tag{35}$$

respectively.

The above formulation and solution are valid in the slip regime (large values of δ) and include both the hydrodynamic solution and its correction due to slip effects. In many occasions, for theoretical and practical purposes, it is convenient to distinguish between these two parts of the solution. This can be achieved by decomposing the velocity u_s as [5,8]

$$u_s(x, y) = u_h(x, y) + \sigma_P u_p(x, y) \tag{36}$$

where u_h is the hydrodynamic part and u_p is the perturbation of the velocity due to slip effects. Eq. (36) is substituted into Eqs. (32) and (33) to yield the following two subproblems. The first one is for u_h, described by

$$\frac{\partial^2 u_h}{\partial x^2} + \frac{\partial^2 u_h}{\partial y^2} = -\delta, \quad \text{with} \quad u_h = 0 \quad \text{at the boundaries} \tag{37}$$

and the second subproblem is for u_p, described by

$$\frac{\partial^2 u_p}{\partial x^2} + \frac{\partial^2 u_p}{\partial y^2} = 0, \quad \text{with} \quad u_p = \frac{1}{\delta}\frac{\partial u_h(x, y)}{\partial n} \quad \text{at the boundaries.} \tag{38}$$

The boundary condition of the second subproblem has been obtained by neglecting terms of $O(\delta^{-1})$. Also, it is noted that the velocities u_h and u_p are of $O(\delta)$ and $O(1)$ respectively. Following the above described analysis it is possible to quantify separately the hydrodynamic and slip effects. For the specific case of an equilateral triangular cross section the two subproblems described by Eqs. (37) and (38) can be solved analytically. The closed form expressions are substituted into Eq. (36) to deduce

$$u_s(x, y) \simeq \frac{\delta}{2}\left(\sqrt{3}xy - x^2 y + \frac{y^3}{3} - y^2\right) + \sigma_P\left(\frac{\sqrt{3}x}{2} + \frac{y}{2} - \frac{x^2}{2} + \frac{y^2}{2} - \sqrt{3}xy + x^2 y - \frac{y^3}{3}\right). \tag{39}$$

At the right-hand side of Eq. (39), the first term is equal to the hydrodynamic velocity u_h, while the quantity inside the parenthesis of the second term is equal to u_p. Finally, integrating Eq. (39), over the equilateral triangular cross section of the flow we find the flow rate

$$G_s \simeq G_h + \sigma_P G_p = \frac{3\delta}{40} + \sigma_P \frac{3}{5}. \tag{40}$$

Eqs. (39) and (40) are approximate of $O(\delta^{-1})$ but this is not a pitfall since in principal slip solutions are valid only for large values of δ. Also, compared to Eqs. (34) and (35), they are simpler and they have the significant advantage that the hydrodynamic and slip effects are clearly distinguished. Even more, the quantities u_p and G_p do not depend on the viscous slip coefficient σ_P. It is obvious that in either case, at the continuum limit, as $\delta \to \infty$, $u_s \to u_h$ and $G_s \to G_h = \frac{3}{40}\delta$.

It is noted that, the semi-analytical result in the free molecular limit ($\delta = 0$) for any triangular cross section and the analytical result in the hydrodynamic limit ($\delta \to \infty$) for the equilateral triangular cross section, are used as benchmarks. The kinetic solution recovers these results at the two limits up to several significant figures. On the other hand the range of validity of the slip solution can be certified only after comparison with the kinetic results.

5. Results and discussion

Calculations have been carried out for various triangular cross sections. Here, we choose to present results for (i) equilateral and (ii) orthogonal isosceles cross sections because they are of particular interest in microfluidics and (iii) for a scalene cross section, with angles ($\hat{\alpha} = 50^o$, $\hat{\beta} = 60^o$, $\hat{\gamma} = 70^o$) in order to demonstrate that the presented kinetic approach can be applied to any triangular cross section. For each channel the dimensionless area A of the cross section is given in Table 1, while the dimensionless perimeter is easily obtained by the relation $\Gamma = 4A$.

Table 1
Dimensionless area of the various triangular cross sections

	Equilateral	Scalene	Orthogonal isosceles
A	$\frac{3\sqrt{3}}{4} = 1.299$	$\simeq 1.326$	$\frac{3}{4} + \frac{\sqrt{2}}{2} = 1.457$

Table 2
Non-dimensional flow rates in terms of δ for various triangular cross sections

δ	G		
	Equilateral	Scalene	Orthogonal isosceles
0	0.930	0.936	0.966
0.001	0.929	0.935	0.965
0.01	0.919	0.925	0.954
0.1	0.872	0.878	0.902
0.25	0.846	0.850	0.872
0.5	0.831	0.835	0.854
0.75	0.829	0.833	0.851
1	0.834	0.837	0.854
1.25	0.841	0.845	0.861
1.5	0.851	0.855	0.870
2	0.876	0.879	0.894
2.5	0.902	0.905	0.920
3	0.933	0.936	0.950
3.5	0.962	0.965	0.980
4	0.996	0.999	0.101 (1)
4.5	0.103 (1)	0.103 (1)	0.105 (1)
5	0.106 (1)	0.107 (1)	0.108 (1)
8	0.127 (1)	0.127 (1)	0.129 (1)
10	0.141 (1)	0.142 (1)	0.143 (1)
15	0.177 (1)	0.178 (1)	0.180 (1)
20	0.214 (1)	0.215 (1)	0.217 (1)
30	0.288 (1)	0.289 (1)	0.292 (1)
40	0.362 (1)	0.363 (1)	0.367 (1)
50	0.437 (1)	0.438 (1)	0.443 (1)

For these three specific cross sections results are provided in the whole range of the rarefaction parameter δ. The accuracy of the results depends on the discretization in the phase space (physical and molecular velocity spaces). In general, for small values of δ we need a large number of discrete velocities, while the physical grid may be coarse. For large values of δ the required number of discrete velocities may be reduced but dense physical grids are important to achieve good accuracy. Depending upon the value of δ and the geometry, the discretization has been progressively refined to ensure grid independent results up to several significant figures. The presented results have been obtained by using a total number of physical lattice points $I = 8 \times 10^4$ when $\delta \leqslant 1.5$, $I = 5 \times 10^5$ when $2 \leqslant \delta \leqslant 8$ and $I = 2 \times 10^6$ when $\delta \geqslant 10$, while the number of discrete velocities is set to $M \times N = 16 \times 300$ when $\delta < 1$ and $M \times N = 16 \times 72$ when $\delta \geqslant 1$. Finally, the termination criterion on the convergence of the iterative process is set equal to 10^{-9}. Based on the above discretization, we were able to recover for all δ and for all cross sections the correct value of the dimensionless mean wall shear stress, given by Eq. (25), up to at least three significant figures within ± 1 at the third one. The same accuracy has been obtained when the numerical results for $\delta = 0$ with the corresponding semi-analytical ones given by Eq. (31) are compared.

Tabulated results for the dimensionless flow rate G for $0 \leqslant \delta \leqslant 50$ and for all three cross sections, are presented in Table 2. The results are considered as accurate to all three significant figures provided within ± 1 at the last figure. It is seen that in all cases the Knudsen minimum is shallow and occurs at about $\delta = 0.75$. Also, the values of G between $\delta = 0$ and $\delta \simeq 0.75$ are reduced about 10% and then for $\delta > 0.75$ they are increased as δ is increased. The qualitative behavior of G in terms of δ is similar to the one observed in circular tubes and in orthogonal ducts with aspect ratios close to one, which are also characterized by shallow Knudsen minimum. In specific applications, once the pressure drop and the exact geometry of the cross section are specified, the corresponding results of Table 2 may be converted to mass flow rates, in a straightforward manner, following the procedure described in Subsection 2.3.

For the specific case of the equilateral cross section, the slip solution obtained by Eq. (35) and the corresponding kinetic solution (second column in Table 2) are plotted in terms of δ, in Fig. 5. It is seen that for $\delta > 10$ the agreement between the two solutions is good. More precisely, by comparing the kinetic and the slip results, it is found that the discrepancy in the slip solution at $\delta = 10$ is 5.3%, at $\delta = 20$ reduces to 2.2%, while at $\delta = 50$ becomes only 1.0%.

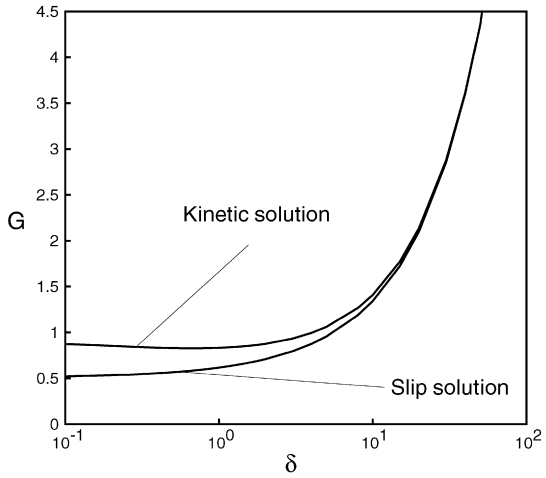

Fig. 5. Comparison between the slip and kinetic solutions in the case of the equilateral triangle cross section.

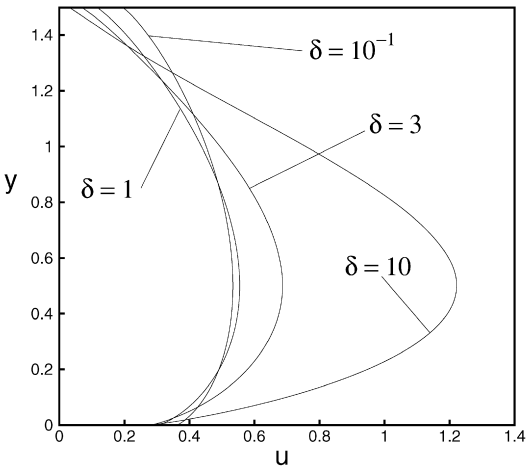

Fig. 6. Velocity profiles for the equilateral triangle along the symmetry axis.

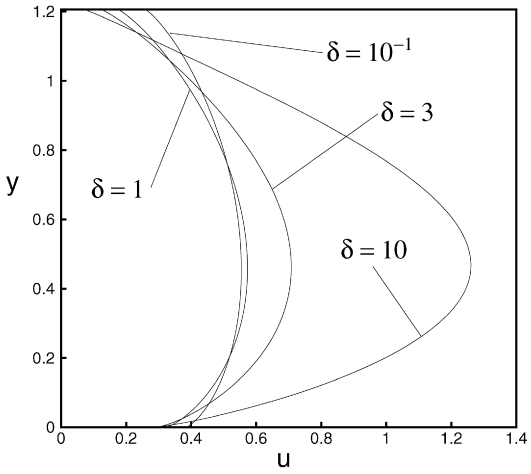

Fig. 7. Velocity profiles for the orthogonal isosceles triangle along the symmetry axis.

These results are indicative for channels of any triangular cross section and therefore, in practical applications one may decide depending upon the required accuracy when a slip solution may be implemented.

We conclude our discussion on this section by presenting some results related to velocity distributions. In Figs. 6 and 7, for the cases of the equilateral and orthogonal isosceles cross sections respectively, the velocity profiles along the symmetry axis are shown. For each cross section the velocity profiles are given for $\delta = 10^{-1}$, 1 and 10. It is clearly seen that at $\delta = 10$ the profiles are parabolic with negligible slip at the walls, while as δ is decreased the velocity profiles are flattening and the slip is increased. Also, for the same cross sections, velocity isolines are presented in Figs. 8 and 9. The position with the maximum velocity can be clearly identified. It is also seen that the velocity slip varies significantly along the walls taking the smallest values at the corners.

6. Concluding remarks

The fully developed flow of a rarefied gas in a channel with a triangular cross section due to an imposed pressure gradient has been investigated implementing a kinetic approach. The BGK kinetic equation, associated with Maxwell diffuse boundary conditions, has been solved by the discrete velocity method. Results for the velocity profiles and the flow rates have been provided for various triangular cross sections in the whole range of the Knudsen number from

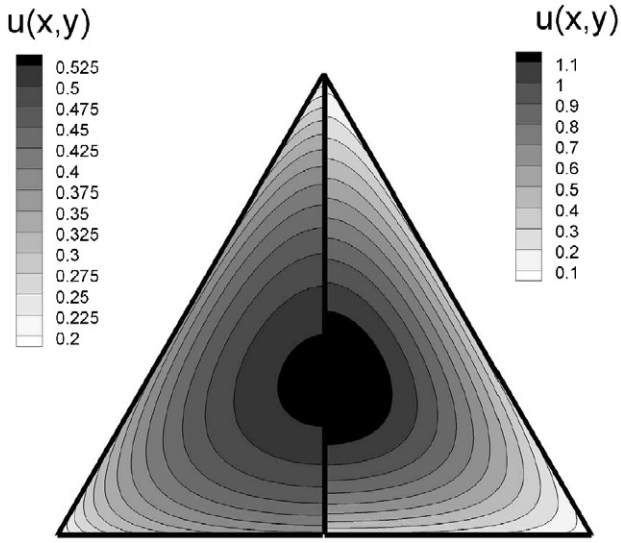

Fig. 8. Velocity isolines for the equilateral triangle with $\delta = 0.1$ (left) and $\delta = 10$ (right).

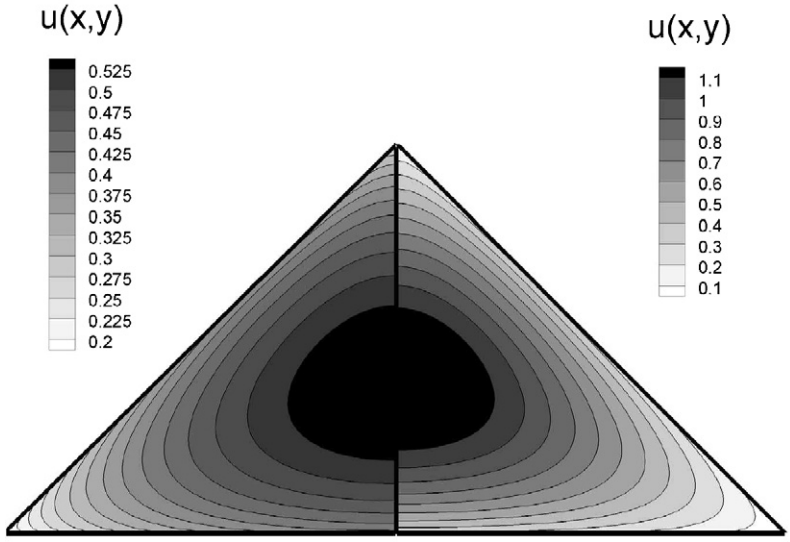

Fig. 9. Velocity isolines for the orthogonal isosceles triangle with $\delta = 0.1$ (left) and $\delta = 10$ (right).

the free molecular limit, through the transition and slip regimes up to the continuum limit. These results are provided for first time in the literature and beyond their theoretical interest, they may be useful in engineering applications as well as in comparisons with experimental results, which as far as the authors are aware of do not exist at this stage.

The successful implementation of the triangular grid elements in the present work may be considered as the first step in an effort to provide kinetic type solutions to rarefied flows in domains with complex geometries and boundaries using adaptive and unstructured grids.

Acknowledgements

Partial support by the Hellenic Ministry of Education through the program on basic research “Pythagoras” is gratefully acknowledged.

References

[1] J.H. Ferziger, H.G. Kaper, Mathematical Theory of Transport Processes in Gases, North-Holland Publishing Company, Amsterdam, 1972.
[2] C. Cercignani, The Boltzmann Equation and its Application, Springer, New York, 1988.
[3] F. Sharipov, V. Seleznev, Data on internal rarefied gas flows, J. Phys. Chem. Ref. Data 27 (3) (1998) 657–706.
[4] K. Aoki, Numerical analysis of rarefied gas flows by finite-difference method, in: E.P. Muntz, D.P. Weaver, D.H. Campbell (Eds.), Rarefied Gas Dynamics, vol. 118, AIAA, Washington, DC, 1989, p. 297.
[5] F. Sharipov, Rarefied gas flow through a long rectangular channel, J. Vac. Sci. Technol. A 17 (5) (1999) 3062–3066.
[6] F. Sharipov, Non-isothermal gas flow through rectangular microchannels, J. Micromech. Microeng. 9 (4) (1999) 394–401.
[7] D. Valougeorgis, S. Naris, Acceleration schemes of the discrete velocity method: Gaseous flows in rectangular microchannels, SIAM J. Sci. Comp. 25 (2003) 534–552.
[8] I. Graur, F. Sharipov, Gas flow through an elliptical tube over the whole range of gas rarefaction, Eur. J. Mech. B Fluids, 10.1016/j.euromechflu.2007.07.003.
[9] F. Sharipov, D. Kalempa, Gaseous mixture flow through a long tube at arbitrary Knudsen number, J. Vac. Sci. Technol. A 20 (3) (2002) 814–822.
[10] S. Naris, D. Valougeorgis, F. Sharipov, D. Kalempa, Flow of gaseous mixtures through rectangular microchannels driven by pressure, temperature and concentration gradients, Phys. Fluids 17 (10) (2005) 100607.
[11] C.Y. Wang, Slip flow in a triangular duct – an exact solution, Z. Angew. Math. Mech. 83 (9) (2003) 629–631.
[12] J. Pitakarrnop, S. Geoffroy, S. Colin, L. Bardas, Slip flow in triangular and trapezoidal microchannels, in: 3rd Microfluidics French Conference – μFlu'06, Proceedings of the Societe Hydrotechnique de France, Toulouse, 2006.
[13] P.L. Bhatnagar, E.P. Gross, M.A. Krook, A model for collision processes in gases, Phys. Rev. 94 (1954) 511–525.
[14] F. Sharipov, V.D. Seleznev, Rarefied gas flow through a long tube at any pressure ratio, J. Vac. Sci. Technol. A 12 (5) (1999) 2933–2935.
[15] S. Naris, D. Valougeorgis, The driven cavity flow over the whole range of the Knudsen number, Phys. Fluids 17 (9) (2005) 907106.
[16] F.M. White, Viscous Fluid Flows, McGraw-Hill, 1974.
[17] D. Valougeorgis, The friction factor of a rarefied gas flow in a circular tube, Phys. Fluids 19 (9) (2007) 091702.